MOLECULAR IMAGING AND BIOLOGY

Mol Imaging Biol (2020)
DOI: 10.1007/s11307-020-01498-5

WMIS World Molecular Imaging Society
esmi European Society for Molecular Imaging

RESEARCH ARTICLE

Volumetric Optoacoustic Tomography Differentiates Myocardial Remodelling

Ivana Ivankovic,[1,2] Xosé Luís Déan-Ben,[1,2] Helena Haas,[3] Melanie A. Kimm,[3] Moritz Wildgruber,[3,4] Daniel Razansky[1,2]

[1]*Faculty of Medicine and Institute of Pharmacology and Toxicology, University of Zurich, Zurich, Switzerland*
[2]*Institute for Biomedical Engineering and Department of Information Technology and Electrical Engineering, ETH Zurich, Zurich, Switzerland*
[3]*Department of Diagnostic and Interventional Radiology, Klinikum Rechts der Isar Technical University of Munich, Munich, Germany*
[4]*Translational Research Imaging Center, Department of Clinical Radiology, Universitätsklinikum Münster, Munster, Germany*

Abstract

Purpose: Myocardial healing following myocardial infarction (MI) is a complex process that is yet to be fully understood. Clinical attempts in regeneration of the injured myocardium using cardiac stem cells faced major challenges, calling for a better understanding of the processes involved at a more basic level in order to foster translation.

Procedures: We examined the feasibility of volumetric optoacoustic tomography (VOT) in studying healing of the myocardium in different models of MI, including permanent occlusion (PO) of the left coronary artery, temporary occlusion (ischemia-reperfusion—I/R) and infarcted c-kit mutants, a genetic mouse model with impaired cardiac healing. Murine hearts were imaged at 100 Hz frame rate using 800 nm excitation wavelength, corresponding to the peak absorption of indocyanine green (ICG) in plasma and the isosbestic point of haemoglobin.

Results: The non-invasive real-time volumetric imaging capabilities of VOT have allowed the detection of significant variations in the pulmonary transit time (PTT), a parameter affected by MI, across different murine models. Upon intravenous injection of ICG, we were able to track alterations in cardiac perfusion in I/R models, which were absent in wild-type (*wt*) PO or kit^{W}/$kit^{W\text{-}v}$ PO mice. The *wt*-PO and I/R models further exhibited irregularities in their cardiac cycles.

Conclusions: Clear differences in the PTT, ICG perfusion and cardiac cycle patterns were identified between the different models and days post MI. Overall, the results highlight the unique capacity of VOT for multi-parametric characterization of morphological and functional changes in murine models of MI.

Key words: Photoacoustic imaging, Myocardial infarction, Reperfusion injury, Pulmonary transit time

Introduction

Ischemia of the myocardium is the most common type of myocardial injury characterised by a prolonged period of reduced blood flow to the heart muscle [1]. Ischemic damage of the heart induces a process of cardiac remodelling, by which extensive morphological, histological and molecular changes occur both within the necrotic and

Moritz Wildgruber and Daniel Razansky contributed equally to this work.
Electronic supplementary material The online version of this article (https://doi.org/10.1007/s11307-020-01498-5) contains supplementary material, which is available to authorized users.

Correspondence to: Daniel Razansky; *e-mail:* daniel.razansky@uzh.ch

healthy myocardium [2]. Until recently, the mammalian heart was assumed to lack regeneration capabilities due to the incapacity of cardiomyocytes to proliferate [3]. Recent studies have shown that resident cardiac stem cells positive for the stem cell factor c-kit possess regenerative properties and can promote the healing response of the myocardium following myocardial infarction (MI) [4]. These observations have fostered preclinical research and clinical studies on stem cell therapies for post-infarct myocardial healing [5–7]. However, while initial clinical trials yielded promising results, these were not substantiated by larger trials involving different types of cell therapies. This called for a better understanding of the fundamental processes involved in cardiac healing post MI and how pluripotent cells affect the healing response. Efforts are therefore being redirected towards improving the preclinical settings in terms of MI models and providing methodological advances to enable more effective *in vivo* observations [8].

Arguably, longitudinal *in vivo* imaging represents the most promising approach for assessing dynamic changes in morphology, function and molecular biology during the healing phase post MI. The existing technologies, such as positron emission tomography and magnetic resonance imaging (MRI) [9], lack key performance metrics required for imaging rapid dynamics in the whole mouse heart, and only regular heartbeat can be observed *via* prospective or retrospective gating [10]. Ultrasound (US) provides a cost-effective and non-invasive approach for imaging of the murine heart in real time. US has been shown to be capable of resolving anatomical changes in response to MI. However, standard 2D cross-sectional US images are prone to artefacts related to cardiac motion, and inter-user variability [11]. While there has been significant development in increasing temporal resolution of 3D US, gating techniques are still required for murine cardiac imaging [12].

Recently, volumetric optoacoustic tomography (VOT) has been suggested as a novel imaging tool for *in vivo* murine heart analysis capable of capturing the entire 3D volume of the beating mouse heart non-invasively and in real- time [13, 14]. Beat-to-beat analysis of healthy and infarcted murine heart models enabled quantifying functional parameters, such as the pulmonary transit time (PTT), defined as the time it takes for blood to pass through the pulmonary circuit connecting the two ventricles [14, 15]. The PTT is estimated by tracking the bolus of a blood pool dye (indocyanine green—ICG) following intravenous (IV) injection [13]. The PTT was found to increase in MI models while an inverse relationship between PTT and time post MI surgery was further observed [14]. Herein, we employed VOT for assessing myocardial regeneration *in vivo* in different MI models. We hypothesise that VOT is able to capture distinct differences of myocardial healing in MI induced *via* permanent occlusion (PO) or ischemia-reperfusion (I/R) as well as infarcted c-kit deficient ($kit^{W}/kit^{W\text{-}v}$) mice, a genetic mouse model with impaired cardiac healing which has been used to study the effects of pluripotent stem cells on the healing of the myocardium [16].

Methods

Acute Murine MI Models: Permanent Occlusion, Reperfusion and c-kit Deficiency

All animal procedures and their care were conducted in conformity with national and international guidelines (EU 2010/63) with approval from the Government of Upper Bavaria and supervised by the Animal Care and Use Committee of the Klinikum Rechts der Isar, Munich, and the Helmholtz Center Munich. Animals were housed in standard animal rooms (12 h light/dark cycle, 50–60 % humidity, 18–23 °C temperature, bedding material) in individually ventilated cage systems (IVS Tecniplast) under specific pathogen-free conditions with free access to water and standard laboratory chow *ad libitum*. Female wild-type albino C57Bl/6J mice (*wt*) ($n = 26$) and WBB6F1-KitW/KitW–v mice ($kit^{W}/kit^{W\text{-}v}$) ($n = 13$) aged 12–14 weeks were used as MI models (Fig. 1a). All mice were intubated and mechanically ventilated for MI surgery after removal of hair from their chest. The intervention was performed by a veterinarian experienced in small animal surgeries. The rib cage was exposed between the 4th and 5th rib. MI induction was based on ligation of the left anterior descending coronary artery (LAD) [17]. In the *wt*-PO model ($n = 13$), MI induction involved consistent closure of the LAD using 8 sutures (Fig. 1a, left panel). The *wt*-I/R model ($n = 8$) involved temporary occlusion of the LAD for approximately 30 min followed by reperfusion (Fig. 1a, middle panel). $kit^{W}/kit^{W\text{-}v}$ mice lack the tyrosine receptor kinase c-kit, which is essential for proliferation, survival, and migration of cardiac stem cells [18]. MI was induced *via* PO in $kit^{W}/kit^{W\text{-}v}$ models ($kit^{W}/kit^{W\text{-}v}$ PO) ($n = 13$) (Fig. 1a, right panel). In all MI models, the rib cage was bound with three stitches and the skin was subsequently closed with transparent surgical glue. Control or non-infarct mice for *wt* models ($n = 9$) and $kit^{W}/kit^{W\text{-}v}$ ($n = 5$) underwent no surgery. VOT imaging was as performed at 3 (3d), 10 (10d), and 21 (21d) days post-surgery (MI) for *wt*-PO (3d, $n = 3$; 10d, $n = 6$, 21d, $n = 4$) and $kit^{W}/kit^{W\text{-}v}$ PO (3d, $n = 4$; 10d, $n = 5$; 21d, $n = 3$) models, while I/R injury was assessed at 3 and 21 days post-surgery (3d, $n = 3$; 21d, $n = 5$).

VOT Imaging Set-up

A detailed description of the VOT imaging set-up is provided elsewhere [14]. In short, the imaging system consists of a 512-element hemispherical array transducer (custom-made Imasonic SaS, Voray, France) with a central US frequency of 5 MHz and ~ 100 % detection bandwidth (Fig. 1b). The VOT images rendered with this array have an almost isotropic resolution of 150 μm within an effective field of view (FOV) of approximately $10 \times 10 \times 10$ mm^3. OA signal excitation was achieved by illuminating the mice with a tuneable (700–900 nm) pulsed (< 10 ns) near-infrared laser (InnoLas Laser GmbH, Krailing, Germany) *via* an optical

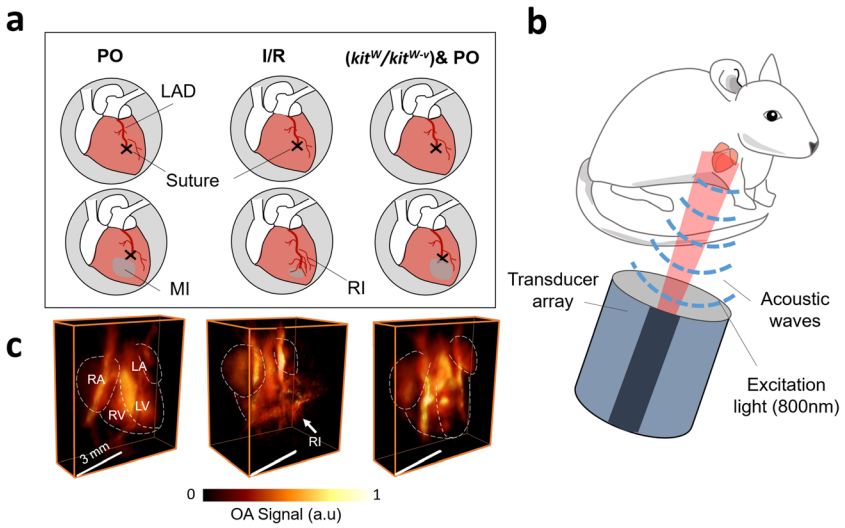

Fig. 1 Schematic of experimental procedure. **a** Procedure of MI induction for varying models with surgical technique and MI outcome. The black cross indicates the suture, the grey shading on left ventricle indicates infarct area and 30 min indicates length of occlusion of LAD (MI; myocardial infarction, LAD; left anterior descending artery, PO; permanent occlusion, I/R; ischemia reperfusion, RI; reperfusion injury). **b** Simplified diagram of ultrasound transducer with fibre output for light delivery to murine heart and curved array for detection of optoacoustic signals. **c** 3D rendered volumes of optoacoustic images of murine hearts corresponding to PO (left), I/R (middle) and *kitW/kitW-v*.

fibre bundle (Ceram Optec GmbH, Bonn Germany) through a central cavity in the transducer array. In the experiments, the wavelength was tuned to 800 nm (peak absorption of ICG in plasma) and the laser was operated at 100 Hz with maximum per-pulse energy of 20 mJ. All 512 OA signals detected by the array elements were simultaneously sampled at 40 megasamples per second by a custom-made data acquisition system (Falkenstein Mikrosysteme GmbH, Taufkirchen, Germany). 3D volumes of $12 \times 12 \times 12$ mm^3 ($120 \times 120 \times 120$ voxels) were reconstructed for each laser pulse using the filtered back projection algorithm [19] without employing signal averaging (Fig. 1c). For this, the raw signals were band-pass filtered between 0.1 and 7 MHz and deconvolved with the impulse response of the transducer elements. For better visualization, a median filter with kernel size $3 \times 3 \times 3$ was applied to the reconstructed images. The graphics processing unit (GPU) implementation of the algorithm further enabled real-time preview during the experiments. All processing steps and analyses were performed in Matlab (version 9.1, R106; MathWorks) and Amira (Zuse Institute, Berlin, Germany) was used for image visualization.

In Vivo Imaging Procedures

For imaging with the VOT imaging set-up, mice were anesthetised with a 2 % isoflurane-medical air mixture (0.8 l/min gas flow). Hair on the chest surrounding the imaged heart region was shaved to minimise image artefacts associated to light and sound attenuation. Mice were then placed in prone position on top of a solid agar block (1.3 % *w*/*v*) filling the volume enclosed by the spherical array pointing upwards. Optimal acoustic coupling for ultrasound transmission was further guaranteed by adding a layer of ultrasound gel between the agar and the skin. The mouse heart was placed into the centre of field of view with the help of real-time image preview [19]. Subsequently, IV injection of 100 nmol ICG (Profiplus Bvba, Korstessem, Belgium) diluted in 50 µl of saline solution was performed and the PTT was measured by tracking the ICG bolus perfusion through the heart with VOT [13]. A total of 5000 volumetric image frames were acquired over 50 s at a wavelength of 800 nm (peak absorbance of ICG) with the injection performed 15 s after beginning the acquisition. Mice were reinjected with the same ICG concentration 10 min after the first acquisition. Imaging of each mouse lasted for about 30 min. The physiological parameters of the animal were constantly monitored throughout the experiments (PhysioSuite, Kent Scientific, Torrington, CO).

PTT in Response to Varying MI Models

The PTT was measured for all models and compared between the different groups. The automated method to extract the PTT has been described previously [14]. In short, tracking the ICG bolus perfusing through the heart was done by tracking the OA signal intensity variations at different points. The PTT was estimated as the difference between the time points corresponding to maximum signal intensities at the right and left ventricles. The value obtained (in seconds) corresponds to the time it takes for the ICG bolus (blood) to complete the pulmonary circuit. All PTT values for each MI

model (*wt* and $kit^{W}/kit^{W\text{-}v}$) were initially compared with non-infarct mice (*wt* and $kit^{W}/kit^{W\text{-}v}$) and then plotted on different days post infarct in order to identify presence of a myocardium remodelling.

In Vivo Analysis of Reperfusion Injury

Analysis of reperfusion injury in *wt*-I/R models was carried out post image reconstruction. Areas located in the region where the LAD was temporary occluded were thoroughly analysed in the VOT images for suspected damage. The hearts of *wt*-I/R models were compared with *wt*-PO models and non-infarcted mice to identify presence of the reperfusion injury, which should be absent in the surgical PO and non-infarcted mice. Perfusion of ICG through the heart and its interaction with the suspected reperfusion injury was further assessed on a beat-to-beat basis for both I/R and PO models. Endothelial dysfunction is a known outcome of reperfusion injury, where the vasculature in the injured area may become leaky. Therefore, the dynamics of the OA signal intensity was measured at the different stages of ICG perfusion to examine whether albumin-bound ICG extravasates due to increased vascular permeability at sites of reperfusion injury.

For validation of increased microvascular permeability for ICG, cryosections containing IV injected ICG obtained 24 h after I/R, were further stained for CD31 (ab28364, Abcam) and detected with an Alexa 647–coupled secondary antibody (Jackson 111-605-144). Mounting media containing DAPI (Thermo Scientific) were used for tissue embedding and visualization of the cell nuclei. All slices were imaged using an Eclipse 50i microscope (Nikon) and NIS-Elements BS 3.22 software (Nikon). Cryosections were H&E stained according to standard protocols and imaged using an Axio Imager M2 microscope (Carl Zeiss) equipped with Zeiss Zen pro 2.0 software (Carl Zeiss).

Cardiac Cycle Characterization

The high temporal resolution of the VOT system enabled analysis of heart activity on a beat-to-beat basis. Irregularities within the cardiac cycle were detected using the interactive viewer View4D (Matlab), where the cardiac cycle could be clearly visualised in the OA signal intensity time profiles. The cardiac cycles in the recorded 5000 volumetric image frames were analysed for all models and time points post MI.

Statistical Analysis

Statistical analysis was carried out on measurements taken from *wt*-PO, *wt*-I/R and $kit^{W}/kit^{W\text{-}v}$ PO and non-infarct models. Boxplots of PTT values were plotted for all MI models and non-infarct models and subsequently compared with each other with a one-way analysis of variance (ANOVA). ANOVA was carried out for assessing differences in heart regeneration of the different models at time points (3, 10 and 21 days) post MI followed by Tukey's *post hoc* test for multiple comparisons. The result of the ANOVA rejects the null hypothesis at 5 % significance level, *i.e.*, p values less than 0.05 were considered to show statistical significance.

Results

PTT Varies Across Different MI Models

PTT values for different mouse models were estimated *via* ICG injection as described in the methods section. The PTTs of the *wt*-PO were significantly longer compared with non-infarct mice (Fig. 2a, $p < 0.0001$). The highest PTT values were observed 3 days post MI and subsequently decreased over time indicating healing of the injured myocardium and functional improvements over 21 days. As the ANOVA analysis indicated significant difference in the PTTs at different days post MI, Tukey *post hoc* tests were performed. *Post hoc* comparisons using the Tukey HSD test indicated that the PTT in mice at 10 days post MI were significantly different from 3 and 21 days post MI ($M = 2.2720$, SD = 0.1878, $p = 0.0017$). For the *wt*-I/R model, which induces a less severe infarct, longer PTTs were also observed compared with the non-infarct mice (Fig. 2b, $p = 0.0206$). However, the decrease in PTT values from day 3 to day 21 post MI showed no statistically significant difference over time ($p = 0.2828$).

PTT values of the $kit^{W}/kit^{W\text{-}v}$ group were analysed to assess effects of the c-kit protein deficiency on heart function and remodelling post MI. $kit^{W}/kit^{W\text{-}v}$ after PO were compared with non-infarcted $kit^{W}/kit^{W\text{-}v}$ mice in addition with *wt*-PO to assess effects of c-kit expression on the functional healing response in MI by VOT. The effect of the deficiency of the c-kit protein on heart function was assessed from VOT measurements of $kit^{W}/kit^{W\text{-}v}$ mice at 3, 10 and 21 days post MI surgery. No improvement in the PTT was measured in $kit^{W}/kit^{W\text{-}v}$ mice after PO with respect to non-infarct $kit^{W}/kit^{W\text{-}v}$ (Fig. 3, $p < 0.0001$). In contrast to what was observed in *wt* mice (Fig. 2a), ventricular function did not recover in $kit^{W}/kit^{W\text{-}v}$ PO mice. VOT-derived PTT values following MI showed no significant differences at different days (3, 10 and 21) post MI (Fig. 3, $p = 0.7079$). These results imply that the lack of proper healing and impaired cardiac function in $kit^{W}/kit^{W\text{-}v}$ mice post MI can accurately be captured by VOT.

VOT Detects ICG Perfusion Through Reperfusion Area

Reperfusion injury is a pathophysiology associated with rapid blood reperfusion following recanalization of an

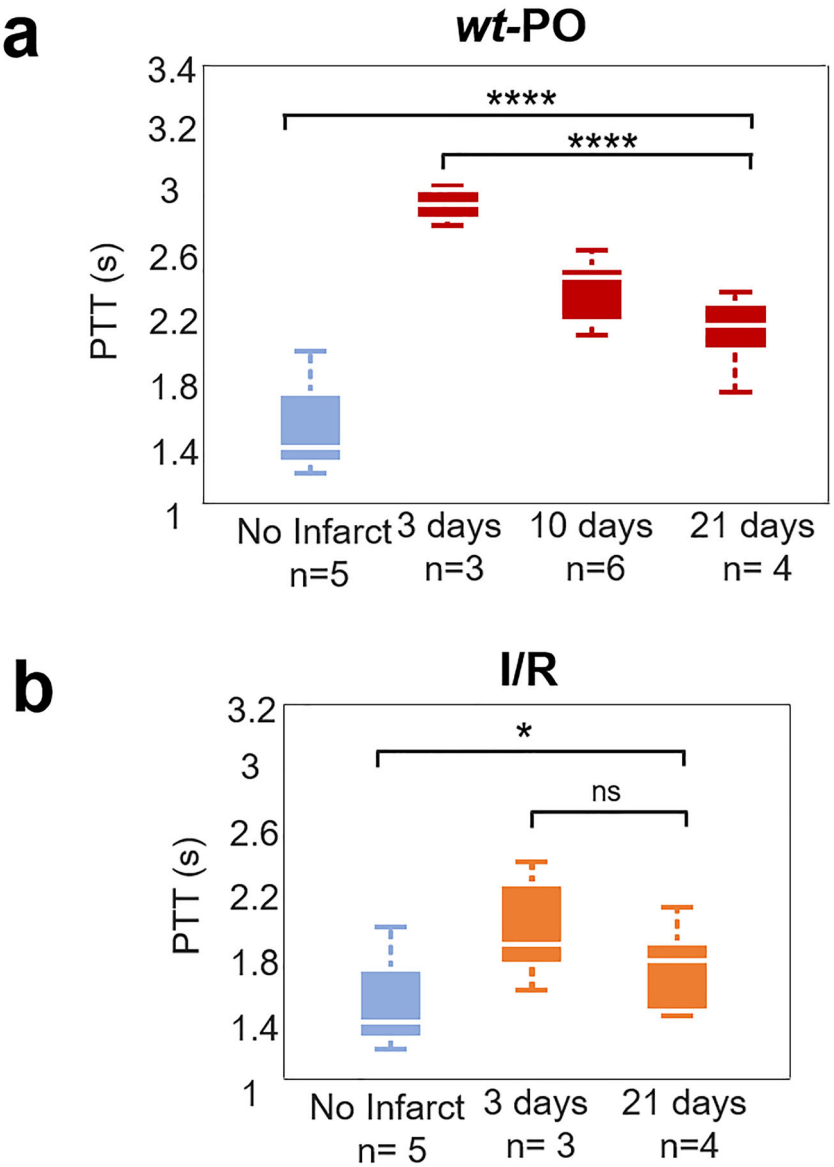

Fig. 2 Pulmonary transit times in PO and I/R models. **a** PTT values represented no MI (blue) and 3, 10 and 21 days post MI for *wt*-PO (red) models. ANOVA analysis showed statistical significance for different days ($p < 0.0001$), suggesting myocardial healing (PTT; pulmonary transit time, PO; permanent occlusion, MI; myocardial infarction). **b** PTT values represented in boxplots for no MI (blue) and I/R models (orange), where the PTT was statistically shorter in no MI mice compared with I/R models ($p = 0.03$) and PTT values represented at 3 and 21 days post MI showed no statistical difference ($p = 0.28$) suggesting no myocardial healing (I/R, ischemic reperfusion).

occluded coronary artery during MI treatment. *wt*-I/R mice showed disrupted vasculature located in regions affected by the temporary LAD ligation (Fig. 1c, white arrows). Similar vasculature was not detected in PO models (*wt* and $kit^{W}/kit^{W\text{-}v}$ mice). The presence of injuries in *wt*-I/R models was corroborated by assessing the ICG perfusion through the suspected injury sites and compared with the PO and non-infarct mice (Fig. 4a). ICG (bound to blood plasma) clearly perfused through structures located on top of the heart (white arrows in Fig. 4a), as manifested by an increase in the OA signal intensity at these points (Fig. 4b). No signal increase was detected in the PO and non-infarct mice, suggesting that the observed absorbing structures do not correspond to disrupted vasculature. On the other hand, the increased VOT signal intensity was maintained for a relatively long time for the selected structures in the *wt*-I/R models, which appears to indicate the presence of leaky vasculature. See supplementary video 1 for visualization of ICG perfusion through the I/R heart. Altered ICG leakage due to increased endothelial permeability was confirmed using fluorescence microscopy (Fig. 4c). Within the infarcted myocardium, ICG (red-coloured) was shown to distribute along the

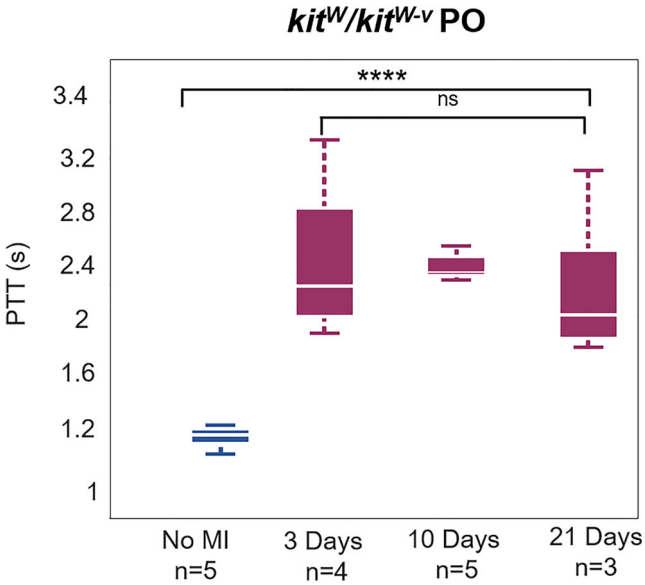

Fig. 3 Pulmonary transit times in *kitW/kitW-v* models. PTT values represented with no MI (blue) and 3, 10 and 21 days post MI (purple). ANOVA analysis showed significant difference in PTT values between no MI and MI models ($p < 0.0001$) and no significant difference in PTT values was detected for 3, 10 and 21 days post MI ($p = 0.7079$) indicating no positive myocardial healing (PTT; pulmonary transit time, MI; myocardial infarction).

microvascular endothelium (green-coloured) into the perivascular space, corroborating the *in vivo* OA–detected ICG signal in reperfusion models.

VOT Detects Arrhythmic Cardiac Dynamic Variations Between PO and I/R Mice

Cardiac cycles were examined with VOT in the *wt*-PO, *wt*-I/R mice as well as in $kit^{W}/kit^{W\text{-}v}$ mice after PO MI. An example of 5000 volumetric OA image frames recorded over 50 s is available in Supplementary Video 2. Irregularities in the cardiac cycle (arrhythmias) were associated to elongated cycles with 82 ± 31 % increase in duration as compared with standard (periodic) cycles (Fig. 5a). In periodic cycles (yellow shade), ventricular activity remained relatively consistent, while ventricular activity was concentrated in diastole in the irregular cycles (Fig. 5a, red shade), occupying approximately 75 % of the cycle length. Cardiac cycle irregularities were detected in all *wt*-PO mice ($n = 21$) and in 37.5 % of *wt*-I/R mice (3 out of 8 mice, $n = 8$), while only periodic cycles were detected in $kit^{W}/kit^{W\text{-}v}$ PO mice ($n = 12$) (Fig. 5b). Longer PTTs were also found in *wt*-I/R mice featuring cardiac cycle irregularities but not in mice with regular cardiac cycles (Fig. 5c, $p < 0.01$). This suggests a high correlation between PTT values and the presence of arrhythmic events, as also observed in hypoxic mouse models [15].

Discussion

The presented results illustrate the advantages of VOT in assessing cardiac dynamics and regeneration following myocardial infarction. Various models of MI are available to help deepen our understanding of the healing response in response to mechanically or genetically induced ischemic injuries. The goal of this study was to assess whether VOT can capture distinct yet subtle differences in myocardial injury and regeneration following MI. The unique capacity of the VOT technique for the simultaneous assessment of cardiac morphology, function, rhythm and vascular morphology *in vivo* and in real time has the potential to offer new insights into the biology of myocardial healing and remodelling.

The PO model involves consistent closure of the LAD, which mimics a clinical acute, untreated MI with relatively large infarct size and worse prognosis [20, 21]. Ligation of the LAD for 30 min in *wt*-I/R models resembles the clinical scenario of coronary revascularization by undergoing rapid treatment in acute MI [21]. The different surgical techniques employed in this study which have imposed varying mechanical stress levels to the heart have resulted in different healing routes post MI. Herein, it was shown that PTT values vary amongst different MI models. In PO models, the PTT was generally longer than in the *wt*-I/R models agreeing with the high severity of the induced injury. The PTT has previously been shown to vary depending upon the time point post MI and its size [14]. The PTT and left ventricular ejection fraction (LVEF) have also been shown to inversely correlate, suggesting that ventricular function can be determined by analysing the PTT. In addition, PTT measurements enabled the assessment of cardio-pulmonary interactions and function under stress [15]. In general, longer PTT values indicate impaired heart function. The normalization of PTT values in the PO model indicate cardiac healing following MI, while no significant changes in PTT values were detected in the I/R model. In support of these findings, no change or improvement in LVEF was detected in patients with reperfused MI and subsequent reperfusion injury [22]. Therefore, although it is generally accepted that I/R models impose less severe infarcts compared with PO models, it appears that the healing capacity in I/R models is altered, which possibly reflects the impact of reperfusion injury.

The regenerative capabilities of c-kit cells in the heart have long been debated. Experimental results have shown that c-kit cells do indeed promote heart regeneration post MI, which have prompted clinical trials yielding controversial outcomes [8, 23]. These inconclusive results call for more preclinical investigations before translating treatment strategies into the clinical setting. For this, advanced imaging techniques with sufficient spatio-temporal resolution for studying the murine heart can be of great value. VOT is capable of capturing the murine heart in real time, non-invasively and volumetrically, posing as an ideal

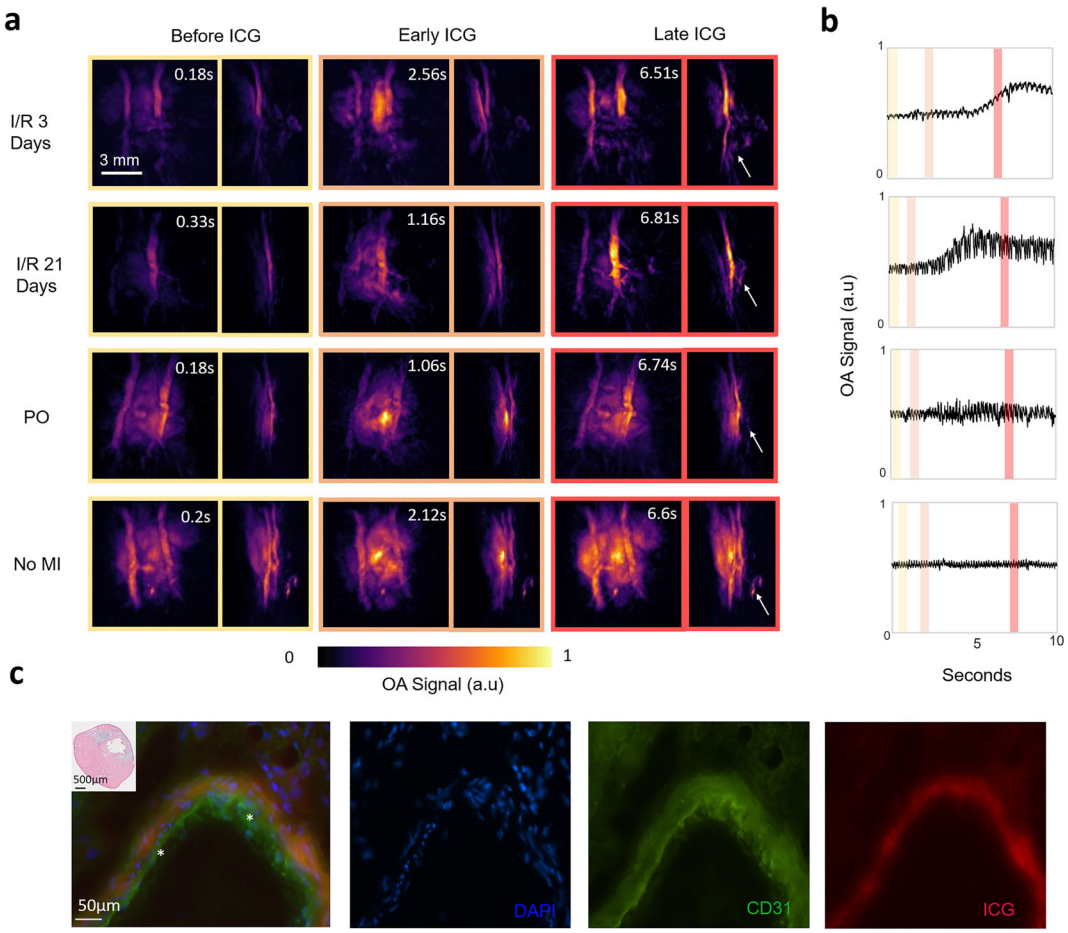

Fig. 4 Reperfusion injury detection. **a** ICG perfusion tracking in I/R (3 and 21 days), PO and no MI models, where before (yellow), early (orange) and late (red) ICG phases are shown. Note white arrows identifying areas where ICG either perfused through (both I/R models) and where ICG did not perfuse through (PO & no MI). Each column of OA MIP images represent coronal views (left) and sagittal views (right) (ICG; indocyanine green, I/R; ischemic reperfusion, PO; permanent occlusion, MI; myocardial infarction). **b** OA signal time intensity plotted at reperfusion injury sites or similar locations are shown for each model over a period of 1000 frames, where different phases of ICG perfusion are depicted (before—yellow, early—orange, late—red). OA images in **a** correspond to the coloured bars in the OA signal time intensity plots. Note how there is a clear increase in OA signal in I/R models and no OA signal change in PO and control models. (OA; optoacoustic). **c** Fluorescence microscopy of infarcted myocardium 24 h following I/R shows a gradient of ICG (red-coloured) spreading across the microvascular endothelium (*CD31 staining in green) into the perivascular space. H&E staining of infarcted myocardium at the mid-ventricular level towards the apex shown in upper left panel.

imaging device to image cardiovascular disease in preclinical models. We tested the sensitivity of VOT by examining different murine MI models. In the $kit^{W}/kit^{W\text{-}v}$ mice, no relevant regeneration of cardiac function was detected by VOT over a 21-day period post permanent LAD ligation. These findings were compared with PO in wild-type mice under identical experimental conditions, where an improvement in the PTT was recorded. This highlights VOT's capacity to assess different degrees of the healing response to MI and emphasises the important role of c-kit cells in cardiac regeneration post MI [23].

The acquired data of the *wt*-I/R model were further investigated to assess the presence of impaired vasculature with increased endothelial permeability, common in reperfusion injuries. The VOT images of the *wt*-I/R hearts presented morphological differences compared with mice without reperfusion injury (PO and non-infarct). Notably, increased leakage of ICG into extravascular space was identified around the infarct area, where reperfusion injury is expected to occur [24]. I/R is known to cause endothelial dysfunction through various mechanisms, where permeability of the endothelium increases following I/R, thus perpetuating myocardial injury [24]. Albumin, which ICG binds to *in vivo* when IV injected, has been previously shown to be a biomarker of vascular permeability as its structure (like other large serum proteins) tends to accumulate in areas of increased vascular permeability [25]. The increased VOT-detected leakage of albumin-bound ICG following IV injection may thus serve as a biomarker of endothelial dysfunction in *wt*-I/R models [26]. These

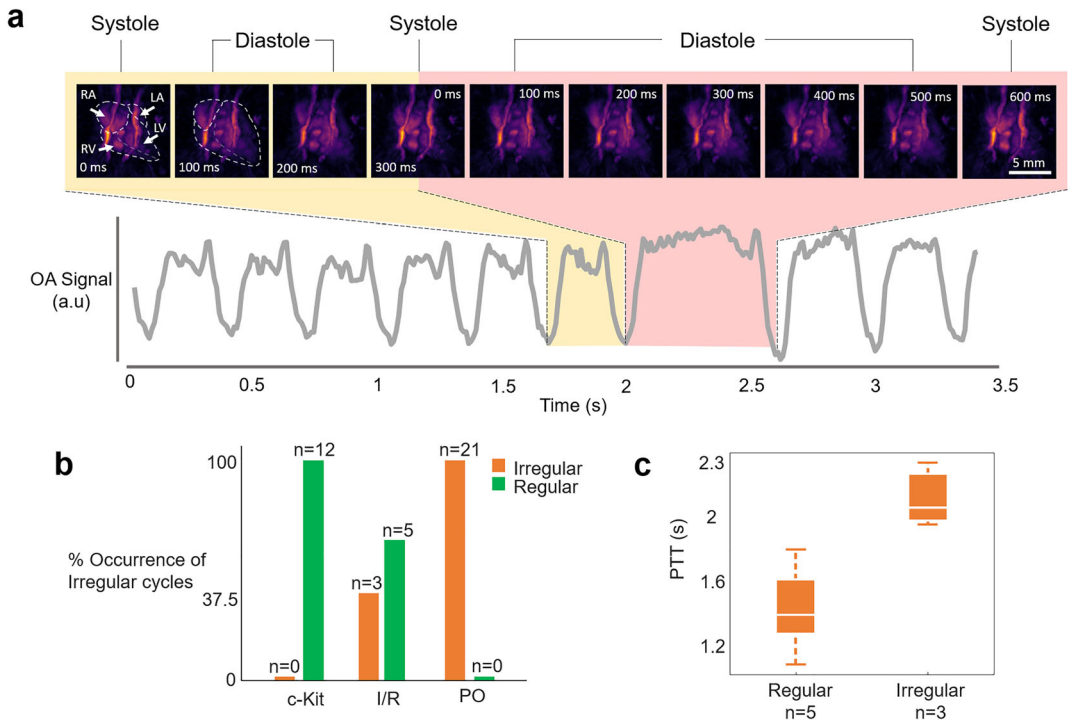

Fig. 5 Cardiac cycle characterization in MI models. **a** OA signal intensity time profile plotted in grey curve where periodic cycles are detected in the beginning followed by irregularity. Above the time plot, individual OA frames of the beating heart across 600 ms are shown, where yellow shading represents a periodic cycle and red shading represents and irregular cycle. Note the differences in systolic and diastolic phases (OA; optoacoustic, RA; right atrium, LA; left atrium, RV; right ventricle, LV; left ventricle). **b** Histogram showing occurrence of cycle irregularities in PO, I/R and $kit^{W}/kit^{W\text{-}v}$ models, where 0 % occurrence was noted in c-kit models, 37.5 % occurrence in I/R models and 100 % occurrence in PO models. Orange colour represents irregular cycles and green represents regular cycles (PO; permanent occlusion, I/R; ischemic reperfusion). **c** Boxplot representation of relationship between PTT values and cardiac cycle trends in I/R models, where a longer PTT was found in models with cycle irregularities ($n = 3$) compared with models with regular cardiac cycles ($n = 5$) ($p = 0.005$).

observations were only recorded in *wt*-I/R models and were not present in wild-type and $kit^{W}/kit^{W\text{-}v}$ mice following PO. The ICG retention in the injured region, as confirmed by fluorescence microscopy, of the I/R hearts similarly follows a previously described schematic on ICG perfusion in MI models [25, 27]. Different phases of ICG perfusion post MI were studied in an I/R rat model. It was shown that in the initial (arterial) phase of perfusion, ICG fills the coronary arterial network of the heart including vasculature with restored blood flow. It was also shown that this is followed by the delayed (capillary) phase, where ICG is detected only in regions of myocardial injury. Disrupted coronary microcirculation was also observed in areas of irreversible reperfusion injury, where excessive leakage of plasma was present [27]. Compared with the unaffected myocardium, the excessive leakage causes retention of ICG, resulting in an OA signal increase measured by VOT. In this study, the entire perfusion cycle of ICG and its retention in the reperfused areas of the myocardium could be detected in real-time and non-invasively. This allowed for fast and direct detection of areas subject to irreversible damage from I/R MI and could serve as a diagnostic tool in classifying the severity of the cardiac injury in those models.

High-frame-rate (100 Hz) imaging with VOT has further allowed for a beat-to-beat analysis of the cardiac cycles. Rapid detection of cycle irregularities was possible due to the true 4D imaging capabilities of VOT, whereby volumetric images of the heart and the OA signal intensity time profiles at different points could simultaneously be analysed. All PO-induced mice presented at least one instance of cycle irregularity in the cardiac cycle post MI, while in *wt*-I/R models irregularities were detected only in 3 out of 8 mice. Notably, no irregularities were observed in the $kit^{W}/kit^{W\text{-}v}$ mice. Cardiac arrhythmias are common in patients following MI, where cycle irregularity can be attributed to slower or faster heart rates [28, 29]. The irregular cycles detected by VOT exhibited almost double the length of the regular periodic cycles, where ventricular activity was extended in the diastolic phase; potentially representing arrhythmic events. The real-time heart motion of the heart is known to serve as an important indicator for the MI assessment [30]. The obtained results suggest that severity of the MI models (with PO considered as the most severe) may dictate frequency of the detected arrhythmic events. However, it remains unclear why no

arrhythmic events were detected in the $kit^{W}/kit^{W\text{-}v}$ mice, and future studies are anticipated to elucidate these findings.

In conclusion, we have shown that dedicated preclinical cardiac VOT imaging can serve as an advanced imaging tool for assessing myocardial injury and regeneration in different MI murine models. VOT is capable of rendering real-time, volumetric and non-invasive data of the murine heart, thus allowing for a comprehensive analysis of the whole heart function under MI stress. Thereby, it has the potential to become a valuable preclinical imaging tool in advancing our understanding of cardiovascular disease.

Compliance with Ethical Standards

Conflict of Interest

The authors declare that they have no conflict of interest.

References

1. Tanai E, Frantz S (2011) Pathophysiology of heart failure. Compr Physiol 6(1):187–214
2. Sutton MGSJ, Sharpe N (2000) Left ventricular remodeling after myocardial infarction: pathophysiology and therapy. Circulation 101(25):2981–2988
3. Kikuchi K, Poss KD (2012) Cardiac regenerative capacity and mechanisms. Annual Rev Cell Dev Biol 28:719–741
4. Urbanek K, Rota M, Cascapera S, Bearzi C, Nascimbene A, De Angelis A, Hosoda T, Chimenti S, Baker M, Limana, Nurzynska D, Torella D, Rotatori F, Rastaldo R, Musso E, Quaini F, Leri A, Kajstura J, Anversa P (2005) Cardiac stem cells possess growth factor-receptor systems that after activation regenerate the infarcted myocardium, improving ventricular function and long-term survival. Circ Res 97(7):663–673
5. Bergmann O, Bhardwaj RD, Bernanrd S, Zdunek S, Barnabe-Heider F, Walsh S, Zupicich J, Alkass K, Burchholz BA, Duird H, Jovinge S, Frisen J (2009) Evidence for cardiomyocyte renewal in humans. Science 324(5923):98–102
6. Madigan M, Atoui R (2018) Therapeutic use of stem cells for myocardial infarction. Bioengineering 5(2):28
7. Behfar A, Crespo-Diaz R, Terzic A, Gersh BJ (2014) Cell therapy for cardiac repair—lessons from clinical trials. Nat Rev Cardiol 11(4):232–246
8. Tompkins BA, Balkan W, Winkler J, Gyöngyösi M, Goliasch G, Fernández-Avilés F, Hare JM (2018) Preclinical studies of stem cell therapy for heart disease. Circ Res 122(7):1006–1020
9. Yu X, Qian C, Chen DY, Dodd SJ, Koretsky AP (2014) Deciphering laminar-specific neural inputs with line-scanning fMRI. Nat Methods 11(1):55–58
10. Lindsey ML, Kassiri Z, Virag JAI, de Castro Brás LE, Scherrer-Crosbie M (2018) Guidelines for measuring cardiac physiology in mice. Am J Physiol-Heart C 314(4):H733–H752
11. Provost J, Papadacci C, Arango JE, Imbault M, Fink M, Gennisson JL, Tanter M, Pernot M (2014) 3D ultrafast ultrasound imaging in vivo. Phys Med Biol 59(19):L1–L13
12. Damen FW, Berman AG, Soepriatna AH, Ellis JM, Buttars SD, Aasa KL, Goergen CJ (2017) High-frequency 4-dimensional ultrasound (4DUS): a reliable method for assessing murine cardiac function. Tomography 3(4):180–187
13. Deán-Ben XL, Ford SJ, Razansky D (2015) High-frame rate four dimensional optoacoustic tomography enables visualization of cardiovascular dynamics and mouse heart perfusion. Sci Rep 5:10133
14. Lin H-CA, Dean-Ben XL, Ivankovic I, Kimm MA, Kosanke K, Haas H, Meier R, Lohofer F, Wildgruber M, Razansky D (2017) Characterization of cardiac dynamics in an acute myocardial infarction model by four-dimensional optoacoustic and magnetic resonance imaging. Theranostics 7(18):4470–4479
15. Ivankovic I, Deán-Ben XL, Lin HCA, Zhang Z, Trautz B, Petry A, Gorlach A, Razansky D (2019) Volumetric optoacoustic tomography enables non-invasive in vivo characterization of impaired heart function in hypoxic conditions. Sci Rep 9(1):8369
16. Marino F, Scalise M, Cianflone E, Mancuso T, Aquila I, Agosti V, Torella M, Paolino D, Mollace V, Nadal-Ginard B, Torella D (2019) Role of c-kit in myocardial regeneration and aging. Front Endocrinol 10
17. Wildgruber M, Bielicki I, Aichler M, Kosanke K, Feuchtinger A, Settles M, Onthank DC, Cesati RR, Robinson SP, Huber AM, Rummeny EJ, Walch AK, Botnar RM (2014) Assessment of myocardial infarction and postinfarction scar remodeling with an elastin-specific magnetic resonance agent. Circ. Cardiovasc Imaging 7(2):321–329
18. Di Siena S, Gimmelli R, Nori SL, Barbagallo F, Campolo F, Dolci S, Feigenbaum L, Lenzi A, Naro F, Cianflone E, Mancuso T, Torella D, Isidori AM, Pellegrini M (2016) Activated c-Kit receptor in the heart promotes cardiac repair and regeneration after injury. Cell Death Dis 7(7):e2317
19. Deán-Ben XL, Ozbek A, Razansky D (2013) Volumetric real-time tracking of peripheral human vasculature with GPU-accelerated three-dimensional optoacoustic tomography. IEEE Trans Med Imaging 32(11):2050–2055
20. Muthuramu I, Lox M, Jacobs F, De Geest B (2014) Permanent ligation of the left anterior descending coronary artery in mice: a model of post-myocardial infarction remodelling and heart failure. Jove-J Vis Exp 94
21. Lindsey ML, Bolli R, Canty JM Jr, Du XJ, Frandogiannis NG, Frantz S, Gourdie RG, Holmes JW, Jones SP, Kloner RA, Lefer DJ, Liao R, Murphy E, Ping P, Przyklenk K, Recchia FA, Schwartz Longacre L, Ripplinger CM, Van Eyk JE, Heusch G (2018) Guidelines for experimental models of myocardial ischemia and infarction. Am J Physiol-Heart C 314(4):H812–H838
22. Ganame J, Messalli G, Dymarkowski S, Rademakers FE, Desmet W, Van de Werf F, Bogaert J (2009) Impact of myocardial haemorrhage on left ventricular function and remodelling in patients with reperfused acute myocardial infarction. Eur Heart J 30(12):1440–1449
23. Hsieh PC et al (2007) Evidence from a genetic fate-mapping study that stem cells refresh adult mammalian cardiomyocytes after injury. Nat Med 13(8):970–974
24. Granger DN, Kvietys PR (2017) Reperfusion therapy—What's with the obstructed, leaky and broken capillaries? Pathophysiology 24(4):213–228
25. Vandoorne K, Addadi Y, Neeman M (2010) Visualizing vascular permeability and lymphatic drainage using labeled serum albumin. Angiogenesis 13(2):75–85
26. Alander JT, Kaartinen I, Laakso A, Pätilä T, Spillmann T, Tuchin VV, Venermo M, Välisuo PA (2012) review of indocyanine green fluorescent imaging in surgery. Int J Biomed Imaging 940585
27. Sonin D, Papayan G, Pochkaeva E, Chefu S, Minasian S, Kurapeev D, Vaage J, Petrishchev N, Galagudza M (2017) In vivo visualization and ex vivo quantification of experimental myocardial infarction by indocyanine green fluorescence imaging. Biomed Opt Express 8(1):151–161
28. Zimetbaum PJ, Josephson ME (2003) Use of the electrocardiogram in acute myocardial infarction. New Engl J Med 348(10):933–940
29. Cohen M, Boiangiu C, Abidi M (2010) Therapy for ST-segment elevation myocardial infarction patients who present late or are ineligible for reperfusion therapy. J Am Coll of Cardiol 55(18):1895–1906
30. Thygesen K, Alpert JS, Jaffe AS, Simoons ML, Chaitman BR, White HD (2012) Third universal definition of myocardial infarction. Circulation 126(16):2020–2035